ELSEVIER

Journal of Power Sources 76 (1998) 153–158

JOURNAL OF POWER SOURCES

Study of lithium insertion in hard carbon made from cotton wool

Emanuel Peled [a,*], Victor Eshkenazi [a], Yuri Rosenberg [b]

[a] *School of Chemistry, Raymond and Beverly Sackler Faculty of Exact Sciences, Tel-Aviv University, Ramat Aviv, 69978 Tel-Aviv, Israel*
[b] *The Wolfson Applied Materials Research Center, Tel-Aviv University, Tel-Aviv, Israel*

Received 29 June 1998; accepted 20 August 1998

Abstract

Hard-carbon materials were made either by one-step or multi-step pyrolysis of cotton cloth between 700 and 1100°C. All carbons have been characterized by gas sorption, X-ray diffraction (XRD) and small-angle X-ray scattering (SAXS) techniques. Two types of carbons have been obtained. One, made by multi-step pyrolysis, has the highest lithium reversible capacity [about 600 (mA h)/g] and two distinct voltage regions: a sloping one between 1.5 and about 0.1 V, called the high-voltage region (HVR), and a horizontal one between 0.1 and 0 V, called the low-voltage plateau (LVP). The other carbons made by the one-step process have only the HVR and less capacity [up to 470 (mA h)/g]. The influence of the current density and temperature on the capacity and degradation rate in both LVP and HVR was checked. We suggest that there are two different modes of lithium insertion: intercalation-like (on both sides of single graphene sheets) at lower potentials and chemical binding to edge carbon atoms at higher potentials vs. lithium reference electrode. A schematic model for lithiated carbon is proposed. © 1998 Elsevier Science S.A. All rights reserved.

Keywords: Hard carbon; Lithium insertion; Lithium-ion batteries

1. Introduction

The lithium-ion batteries in use today have graphitic or hard-carbon anodes with a practical reversible lithium capacity of about 300 (mA h)/g. In the past decade, various precursors have been examined as sources of hard (disordered) carbons. A wide spectrum of examples was investigated, for instance, in the work of Xing et al. [1]. Most of those materials reached reversible capacities of up to 600 (mA h)/g while cycled at constant current between −0.02 and 3.0 V vs. Li/Li^+ (i.e., the cycling procedure includes lithium metal plating and subsequent stripping). Shi et al. [2] cycled similar carbons at constant current between 0.01 and 2.0 V, but found no carbon with a reversible capacity exceeding 250 (mA h)/g. Such a disagreement, among other reasons, justifies further study of carbons from this group.

Different mechanisms have been proposed to describe lithium insertion into carbonaceous materials. Most of them deal with specific carbons with no claims to universality. The focus of these models is the explanation of the extra capacity of lithium over the common value of 372 (mA h)/g C for LiC_6 in ideal graphite. According to Ishikawa et al. [3], lithium exists between graphene layers in 'pseudo isotropic' hard carbon and forms clusters in fine micropores as well. Sato et al. [4] proposed LiC_2 as a final formula for fully lithiated *p*-phenylene based carbon, which implies covalent molecules, Li_2, in addition to the lithium ions. Mabuchi et al. [5] postulate the storage of lithium in the form of lithium ion clusters in the carbon cavities of Mesocarbon Microbeads heat-treated below 1000°C. In the soft carbon of Yazami and Deschamps [6,7], up to three lithium layers are supposedly formed on each face of the graphene units. According to Zheng et al. [8–10], lithium atoms bind in the vicinity of the edge hydrogen atoms, i.e., a correlation exists between the amount of inserted lithium and hydrogen content both for soft and hard carbons. A computational model of the same idea has been described by Papanek et al. [11]. Its main postulate is the conversion of the edge carbon atom from the sp^2 to the sp^3 state as a result of the binding of lithium and hydrogen to the same carbon atom. Chemical bond formation between C and Li including substitution of edge

* Corresponding author. Tel.: +972-3-6408-751; Fax: +972-3-6409-293

0378-7753/98/$19.00 © 1998 Elsevier Science S.A. All rights reserved.
PII: S0378-7753(98)00148-7

H by Li and binding of Li to edge carbon radical was proposed by Peled et al. [12] at first for graphites and subsequently for carbons as well [13].

The most accepted model so far is the 'house of cards' model of Zheng et al. [8,9] and Dahn et al. [14], proposed for hard carbons. The extra capacity of lithium is attributed to adsorption on the internal surfaces of nanopores, which are formed by graphene sheets, or 'cards'. Subsequently, Dahn et al. [15] proposed the 'falling cards' as a more common conceptual model for microporous carbons. This modification of the 'house of cards' is invoked to explain the decrease in lithium insertion capacity with rise in temperature. As a carbon is heated, sufficient energy may be provided to break the links between adjacent sheets, allowing some to rotate into parallel orientations. Thus they may 'fall', eliminating non-parallel stacking and reducing the total number of pores. Lately the 'falling cards' model has been criticized by Sorek et al. [16]. In their so-called 'potato-chips' model, edge-connected graphene fragments are proposed instead of isolated single 'cards' and translation is considered to be the process more likely responsible for the rearrangement of carbons during heating.

In this work we have tried to find a correlation between physicochemical properties (surface area, pore size distribution, structure) and lithium reversible (Q_r,) and irreversible capacity (Q_{ir}) of cotton-derived hard-carbon materials. In addition, we have attempted to explain the lithium insertion process into carbons.

2. Experimental

A cotton cloth precursor was pyrolysed by two different procedures.

(A) One-step: 3-h heating and 1-h dwell time under flow of about 500 cm^3/min of the argon/hydrogen mixture (92/8 by volume). Precursor weight varied between 40 and 80 g. Five samples were prepared in this way up to final temperatures of 700, 800, 900, 1000, and 1100°C. The materials obtained were marked by these numbers respectively and the overall group was called Group A.

B. Multi-step: heating up to 500°C, 1 h dwell time, cooling, grinding, subsequent heating to 1000°C, 1 h dwell time and cooling under argon/hydrogen. About 70 g of precursor were inserted in the first step and 4.5 g in the second. The final material was marked 1000B.

The carbons, thus obtained, were mixed with 5% PVDF and 5% Shawinigan Black and spread on copper foil to give electrodes of about 30 μm thickness. Electrochemical cells were assembled with these electrodes and lithium counter electrodes pressed on a nickel grid. In order to rule out 'electrolyte effect', two kinds of electrolytes were used: (1) 1.2 M $LiAsF_6$ (FMC) in 1:2 EC:DEC (both Grant Chemicals); (2) 1 M $LiPF_6$ in 1:1 EC:DEC solution (Merck). The cells containing the former were cycled from 0.00 to 2.00 V, and the ones with the latter between 0.00 and 1.50 V. Cells with carbon 1000B were run with the former electrolyte only. Cells with carbons 700–1100 were made with both electrolytes. Cycling tests were performed at different current densities and temperatures with the use of a 16-bit MACCOR 2000 Battery Tester.

X-ray diffraction (XRD) characterization was performed on a Scintag θ:θ Diffractometer equipped with a liquid nitrogen cooled Ge solid state detector. Cu-Kα radiation was used. Small-angle X-ray scattering (SAXS) studies were carried out with the same instrument in a transmission mode using a sample holder with 40 μm Kapton foil windows.

All the carbons were analyzed by a NOVA 2200 gas sorption analyzer (Quantachrome) at 77 K with nitrogen (99.999%) as an adsorbate. Outgassing of about 14 h at 300°C preceded each analysis.

3. Results and discussion

When an organic precursor is exposed to pyrolysis, many factors affect the overall process: type, amount and homogeneity of the starting material, heating rate, final temperature, gas flow rate (or vacuum) and additional procedures (pressing, binding, grinding, etc). To avoid eventual oxidation by impurities or air from leakages, a gas mixture containing 8% v/v hydrogen was used. The capacities of the carbons obtained by the one-step mode (Table 1) were substantially smaller than those reported by Xing et al. [1], and their specific area substantially larger (Table 2). The reasons for this difference is not fully clear. It may be due to the greater amount of precursor we started with (40–80 g) compared with Zheng et al., who usually began with 10 g or less [8]. In our case the abundant pyrolysis products may attack the newly formed carbon, thus causing an increase in the surface area and destruction of the carbon bulk. In order to avoid this we checked the multi-step mode by which carbon 1000B was made.

Table 1
Cycling, XRD and SAXS data for the studied samples

Carbon code	Q_r^a [(mA h)/g]	Q_r^b [(mA h)/g]	R_s (Å)	Intercept	R
700	180	350	4.50	2.626	2.21
800	376	460	6.00	3.605	2.23
900	346	435	5.53	3.174	2.27
1000	312	365	6.08	3.258	2.62
1100	298	310	6.75	3.913	2.76
1000B	410	610	8.19	5.301	2.50

[a]At room temperature and $i = 50\ \mu A/cm^2$.
[b]At 50°C (60°C for 1000B) and $i = 25\ \mu A/cm^2$.

Table 2
Gas sorption data for the studied samples

Carbon code	Cumulative pore volume $[(cm^3/g) \times 10^{-3}]$			S_{BET} (m^2/g)	Q_{ir}^a [(mA h)/g]
	< 35 Å	35–55 Å	> 55 Å		
700	84	26	6	515	490
800	69	22	7	510	410
900	95	35	11	555	560
1000	104	36	11	540	480
1100	87	31	14	450	460
1000B	12	13	15	41	130

[a]At room temperature and $i = 50\ \mu A/cm^2$.

The charge–discharge curve of carbon 1000B (Fig. 1) consists of two parts, marked as LVP (low-voltage plateau) and HVR (high-voltage region). At room temperature the capacities associated with LVP and HVR were 182 (mA h)/g and 246 (mA h)/g, respectively. When cycled at 60°C, the LVP capacity increased to 244 (mA h)/g (an increase of 34%) and that of HVR to 340 (mA h)/g (38%).

The degradation rate of the LVP is greater than that of the HVR. At the beginning of the 60°C cycling test the LVP capacity was about 41% of the overall capacity and after nine cycles it dropped to about 10%. The current density significantly affects the reversible capacity of carbon 1000B: the increase of Q_r from 300 to 407 (mA h)/g with decrease of the current density from 50 to 10 $\mu A/cm^2$ indicates mass-transport or kinetic problems.

In Group A carbons LVP is absent both at room and at elevated temperatures (Fig. 2, carbon 800 taken as an example). No significant capacity changes were observed when the cells were cycled in different electrolytes. Over the voltage range of 1.50–2.00 V there is no lithium capacity, so all the cells are definitely comparable.

Table 1 summarizes cycling, XRD and SAXS data for all the carbons. It can be seen that the reversible capacity of carbon 800 is maximal for Group A. The significant increase in Q_r of most samples when cycled at 50°C also testifies to a serious kinetic problem in getting the full capacities of these carbons as is the case for carbon 1000B.

The characteristic pore radius R_s was derived from SAXS data according to the formula of Guinier and Fournier [17]:

$$I(q) = CNV^2 \exp\left[-1/3(qR_g)^2\right],$$

where $I(q)$ is the SAXS intensity, R_g is the radius of gyration of randomly distributed spherical pores, N is the number of pores, V is their volume, C is a proportion coefficient, and q is the wave-vector given by

$$q = 4\pi \sin\theta/\lambda,$$

where λ is the wave length and 2θ is the scattering angle.

The Guinier plots (log $I(q)$ vs. q^2) for carbons 1000 and 1000B are shown in Fig. 3. The pore radius R_s is calculated from the plot, taking $R_g = 0.7746 R_s$. For carbon 1000B, R_s is found to be 8.2 Å, which is larger than reported [1] for carbohydrates. For carbons 700–1000 the values are comparable (5.5–6.1 Å). A small-angle neutron scattering (SANS) measurement of carbon 1100, performed by Sorek [18] gave $R_s = 7.23$ Å as opposed to 6.75 Å from SAXS.

An empirical factor, '*R*', related to the (002) XRD peak-to-background ratio, was introduced by Liu et al. [19] in order to characterize the fraction of organized carbon regions in the samples. Xing et al. [1] found that the

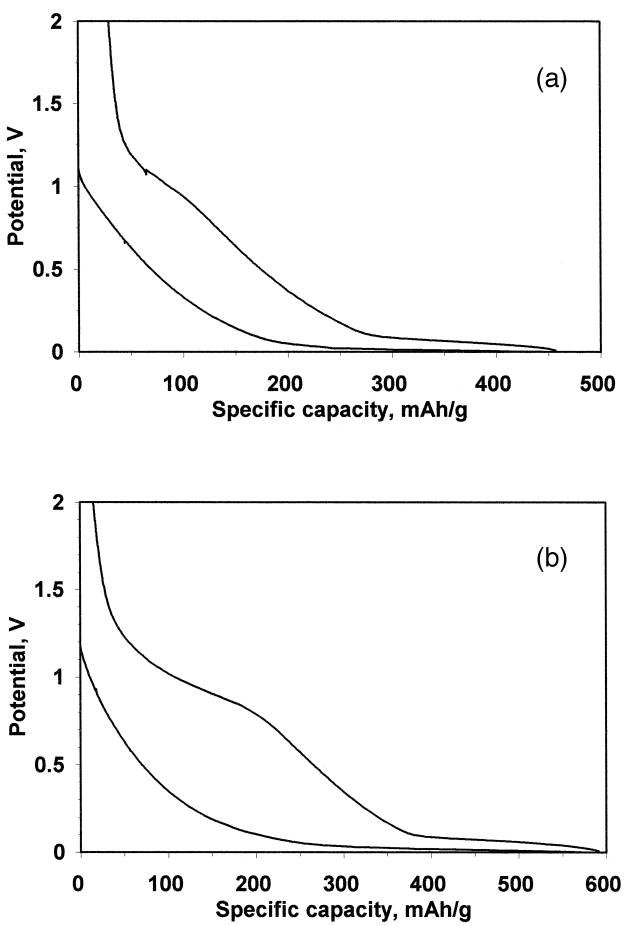

Fig. 1. Charge–discharge curves for carbon 1000B: (a) at room temperature; (b) at 60°C.

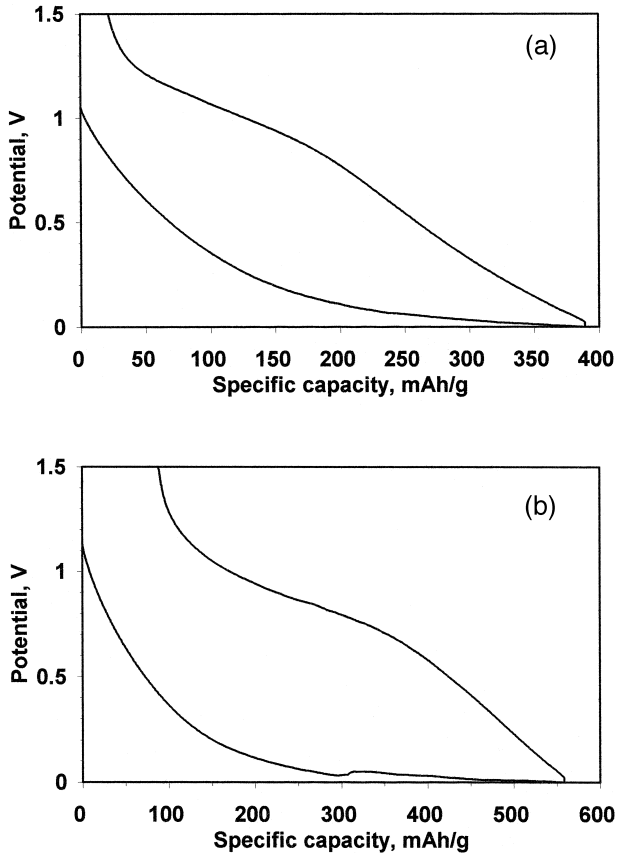

Fig. 2. Charge–discharge curves for carbon 800: (a) at room temperature; (b) at 50°C.

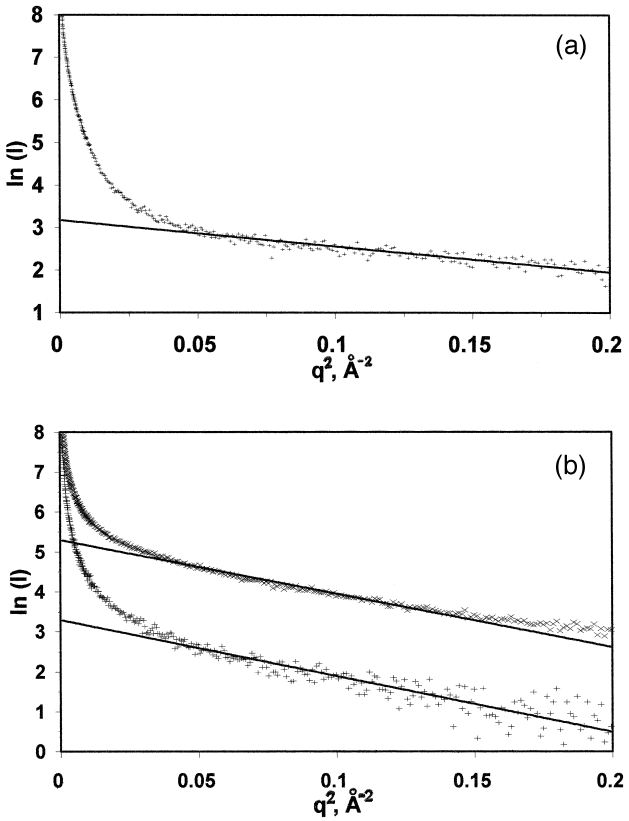

Fig. 3. Guinier plots for: (a) carbon 1000; (b) carbon 1000B, the upper line indicates pristine sample and the bottom line sample after cycling.

smaller the value of R (i.e., the less ordered the carbon), the higher the lithium capacity. Factor R depends on the value of parameter A (Fig. 4), which in its turn depends strongly on the background level. In order to reduce the non-sample scattering, a low-background quartz plate was used as a sample holder. Obviously, in the presence of a large number of scatterers in the sample, the SAXS tail contribution to the background might be significantly high. In our opinion, this heavy SAXS tail causes the increase in background of carbon 1000B and thus the decrease in R. Within Group A carbons the parameter R increases with pyrolysis temperature as expected, but no clear correlation was found between it and Q_r.

For the pore-size distribution the Barrett–Joyner–Halenda (BJH) method [20] was used. Although they are significantly different in their performance, all of the materials exhibit a characteristic peak at about 40–42 Å (Fig. 5).

The most important data obtained from gas-sorption measurements are included in Table 2.

The most prominent differences between Group A carbons and carbon 1000B (except for the existence of the LVP) are enumerated below.

(1) 1000B has BET surface area smaller by an order of magnitude.

(2) Its irreversible capacity is smaller by a factor of 3, which is mostly due to 1.

(3) Its pore volumes in the ranges < 35 Å, 35–55 Å, and > 55 Å are almost identical, while the other carbons have a very large cumulative volume of small pores.

(4) The SAXS intercept of 1000B is substantially greater, i.e., a large number of closed (for nitrogen) pores exist in its bulk. Additional SAXS and BET measurements of this material were performed after cycling. The slope of the Guinier plot did not change, which means that the dimensions of the scatterers (pores) remained the same, but

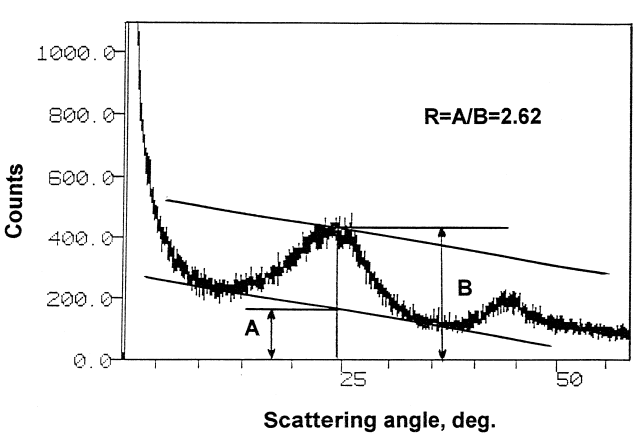

Fig. 4. XRD spectrum and R factor for carbon 1000.

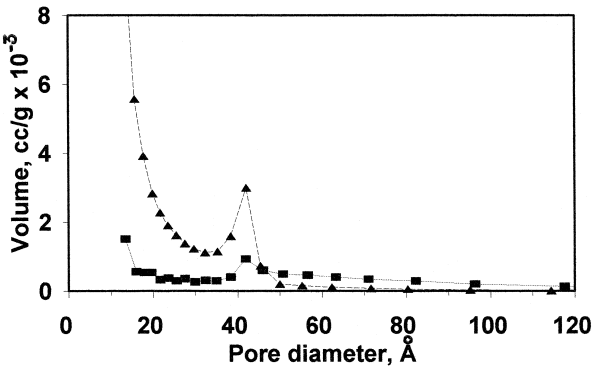

Fig. 5. Barrett–Joyner–Halenda pore size distribution for carbons 800 (▲) and 1000B (■).

the intercept decreased from 5.3 to 3.3, indicating a lower number of scatterers and thus a lower total pore volume. The BET surface area decreased from 41 m^2/g to about 5 m^2/g, which is a result of solid electrolyte interphase (SEI) formation.

We assume that the HVR capacity is associated with edge carbons according to the following processes:

Cleavage of strained C–C bonds (e.g., between two graphene units) and termination of emerging radical edges by Li^+ [Eq. (1)]. This process involves changes in the carbon structure:

$$\text{``C–C''} + 2Li^+ + 2e^- \Leftrightarrow 2C\text{–}Li \quad (1)$$

Reaction between lithium and edge carbon located in sites to which solvent molecules cannot approach (closed or narrow-necked pores):

$$C\cdot + Li^+ + e^- \Leftrightarrow C\text{–}Li \qquad (E^o \sim 0.3\ V) \quad (2)$$

Substitution of terminal H by Li [Eqs. (3) and (4)]. Two main substitution reactions can occur:

$$C\text{–}H + 2Li^+ + 2e^- \Leftrightarrow C\text{–}Li + LiH \qquad (E^o \sim 0.6\ V) \quad (3)$$

$$C\text{–}H + Li^+ + e^- \Leftrightarrow C\text{–}Li + 1/2H_2 \qquad (E^o \sim 0.5\ V) \quad (4)$$

In reactions [2–4] there is no deformation of the carbon structure. These processes have been suggested for oxidized graphite [12]. The C–Li bond obtained by [1–4] has a relatively strong ionic character.

LVP is attributable to a doping process, mainly in the closed pores. Lithium ions migrate into the carbon and occupy appropriate sites above and below the graphene sheets. Interaction between Li^+ and π-orbitals of the carbon, causing partial compensation of the positive charge of the former, does not require crossing of high energetic barriers, thus only a small overpotential accompanies this process, in contrast to those corresponding to the HVR. It seems possible that doping, like intercalation in graphites, involves some structural rearrangement in the carbon bulk. This can explain the faster degradation rate of lithium insertion capacity in the LVP. In a recent ^7Li NMR study Dai et al. [21] found that the lithium in the LVP is less ionic than that in the HVR: the LVP lithium of carbon 1000B has a chemical shift of 50 ppm (similar to 34–44 ppm for intercalated graphite), while the HVR lithium has a shift of only 17 ppm (typical for a Li–C covalent bond).

These results are in agreement with the model schematically described in Fig. 6. The lithium atoms, which are not directly bonded to carbon, are positioned below or above the plane of the sheet. They correspond to the LVP, while the directly bonded lithium atoms are assigned to the HVR.

The overpotential of the HVR (so-called hysteresis) is much larger than that of the LVP (Figs. 1 and 2). This difference is attributed to slower diffusion in the HVR. Since doping is the main process responsible for the LVP, many sites are occupied by Li^+ and diffusion on the nano-size graphene sheets is rapid (as in graphite). In the HVR the contribution of doping is minor, the concentration of Li^+ on these graphene sheets is extremely low and this diffusion path is considered to be very slow. The available diffusion process in the HVR is the hopping of Li^+ from one edge site to its neighbouring site.

It is not clear yet why carbons with LVP can be obtained only at 900 1100°C (see, for example, Zheng et al. [8] and Satoh et al. [22]). As was mentioned above, this region can be correlated with the closed small features (pores or voids) in carbon 1000B. It is believed that these voids (about 1.5–2 nm in diameter) are formed between non-parallel single graphene sheets as described by Zheng et al. [8]. At temperatures below 900°C the sheets are too small, and the adsorption of lithium is not favoured energetically. Above 1100°C the sheets either collapse, forming larger voids (falling-cards model [15]) or begin to 'surf', decreasing the number of voids (potato-chips model

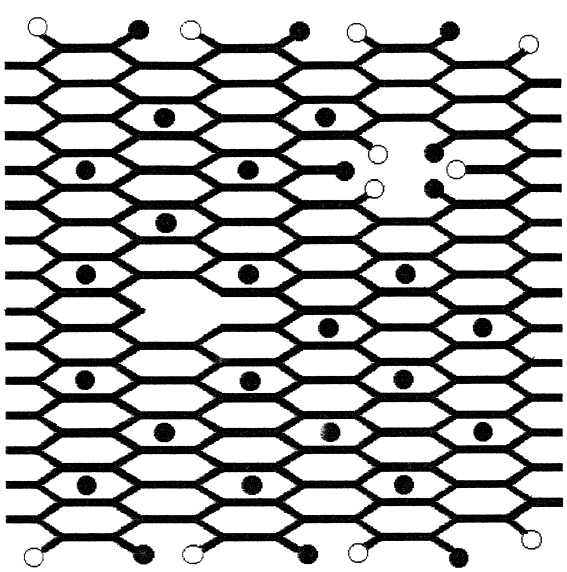

Fig. 6. Schematic description of partially lithiated carbon: Li atoms (●); H atoms (○).

[16]). In both models the fraction of single graphene sheets in the carbon bulk decreases.

According to the BET area, the carbons from group A have too many open pores. The SAXS intensities of these carbons indicate few, if any, closed pores. The typical diameter of the scatterers in this group is smaller than 1.4 nm. This means that the graphene sheets that form the voids are small and do not allow doping of lithium. Another reason for the absence of LVP in these carbons can be the great number of defects in the graphene sheets caused by the rapid pyrolysis of a relatively large amount of precursor.

4. Conclusions

(1) We ascribe the sloped part of the charge–discharge curve of our carbons (from 0.1 to about 1.5 V vs. Li/Li^+) to Li–C covalent bond formation. This process occurs at the edge sites of the carbon particles.

(2) We ascribe the flat part of the same curve (between 0.1 and 0.0 V) to an intercalation-like process, in which lithium adsorbs on both sides of single unparallel graphene sheets, which form small voids (typically 1.5–2.0 nm in diameter).

(3) Multi-step pyrolysis like that described above can help to get single sheets morphology and to decrease the specific surface area of the final product and thus its irreversible capacity.

Acknowledgements

The authors would like to thank the Israel Ministry of Science for financial support.

References

[1] W. Xing, J.S. Xue, T. Zheng, A. Gibaud, J.R. Dahn, J. Electrochem. Soc. 143 (1996) 3482.
[2] H. Shi, J. Barker, P. Liu, 190th Electrochemical Society Meeting, San Antonio, Oct. 1996, p. 1053.
[3] M. Ishikawa, N. Sonobe, H. Chuman, T. Iwasaki, 2B10, 35th Battery Symposium in Japan, Nov. 1994, p. 49.
[4] K. Sato, M. Noguchi, A. Demachi, N. Oki, M. Endo, Science 264 (1994) 556.
[5] A. Mabuchi, K. Tokumitsu, H. Fujimoto, T. Kasuh, J. Electrochem. Soc. 142 (1995) 1041.
[6] R. Yazami, M. Deschamps, 13th International Seminar on Primary and Secondary Battery Technology and Application, FL, March 1996.
[7] R. Yazami, M. Deschamps, 8th International Meeting Lithium Batteries, Nagoya, June 1996, p. 188.
[8] T. Zheng, Y. Liu, E.W. Fuller, S. Tseng, U. von Sacken, J.R. Dahn, J. Electrochem. Soc. 142 (1995) 2581.
[9] T. Zheng, J.S. Xue, J.R. Dahn, Chem. Mater. 8 (1996) 389.
[10] T. Zheng, W.R. McKinnon, J.R. Dahn, J. Electrochem. Soc. 143 (1996) 2137.
[11] P. Papanek, M. Radosavljević, J. Fischer, Chem. Mater. 8 (1996) 1519.
[12] E. Peled, C. Menachem, D. Bar-Tow, A. Melman, J. Electrochem. Soc. 143 (1996) L4.
[13] V. Eshkenazi, E. Peled, 190th Electrochemical Society Meeting, San Antonio, Oct. 1996, p. 1051.
[14] J.R. Dahn, T. Zheng, Y. Liu, J.S. Xue, Science 270 (1995) 590.
[15] J.R. Dahn, W. Xing, Y. Gao, submitted to Science.
[16] Y. Sorek, P. Zhou, J.E. Fischer, T. Ishihara, submitted to Carbon.
[17] A. Guinier, G. Fournier, Small-Angle Scattering of X-rays, Wiley, New York, 1955.
[18] Y. Sorek, private communication.
[19] Y. Liu, J.S. Xue, T. Zheng, J.R. Dahn, Carbon 34 (1996) 193.
[20] E. Barrett, L. Joyner, P. Halenda, J. Amer. Chem. Soc. 73 (1951) 373.
[21] Y. Dai, Y. Wang, V. Eshkenazi, E. Peled, S.G. Greenbaum, J. Electrochem. Soc. 145 (1998) 1179.
[22] A. Satoh, M. Oguchi, H. Sasaki, N. Takami, T. Ohsaki, 2A01, 37th Battery Symposium in Japan, Sep. 1996, p. 111.